

PARALLEL EULERIAN METHODS FOR FLOWS WITH ELASTIC MEMBRANES*

JUDITH C. HILL[†], NOEL WALKINGTON[‡], AND OMAR GHATTAS[§]

Abstract. We propose and study parallel numerical algorithms for simulation of flows with elastic membranes, such as red blood cells. The challenges of modeling such flows include accurately resolving the interface motion and enforcing the appropriate interface mechanics. We propose a phase field Eulerian method for implicitly capturing the location of the dynamic interface between two fluids. In addition, for flows with elastic membranes separating the fluids, we present a phase field formulation for the membrane stresses. The method we propose avoids the computational geometry complexities associated with fully Lagrangian or front-tracking Eulerian methods. These complexities are particularly pronounced on parallel computers. The phase field formulation is discretized by a combined continuous/discontinuous Galerkin method, which lends itself to an inherently parallel implementation. We present a block Schur-complement preconditioner for the coupled membrane-flow system that neutralizes the ill-conditioning due to disparate material properties. Parallel performance results demonstrate the efficacy of this preconditioner.

1. Introduction and motivation. In this paper we propose and study parallel numerical algorithms for simulation of flows with elastic interfaces. Such problems belong to the general class of flows of multi-fluids. Modeling such flows necessitates resolution of dynamic interfaces, which presents mathematical, numerical, and computational challenges. Physical examples of such flows include the mixing of two immiscible fluids, the flow of blood cells through capillaries and arteries, and the transport of contaminants in groundwater.

Our interest is in cell-scale simulations of blood flow. Blood is composed primarily of red blood cells (RBCs) and plasma. An RBC can be modeled as a Newtonian fluid (hemoglobin) encapsulated by an elastic membrane, while plasma is essentially Newtonian. Other components of blood, such as white blood cells and platelets, occupy a negligible volume fraction of blood. This inhomogeneous mixture of RBCs in plasma can exhibit such macroscopic non-Newtonian behavior as shear-thinning, viscoelasticity, shear-induced anisotropy, and phase separation. This behavior could be predicted by cell-scale simulations that resolve individual cell deformations and interactions with the surrounding plasma.

One of the motivating problems for cell-scale simulations of blood flow is the design of ventricular assist devices (VADs), for which it is crucial to understand blood damage at the cellular level [4, 5]. Current blood flow models used in the design of artificial hearts and heart-assist devices are macroscopic, treating blood as a homogeneous continuum. Rather than resolve individual cellular interactions, macroscopic blood flow models distribute the cell-scale effects into the continuum. However, continuum models of cellular interactions, such as the red blood cell-plasma interface forces, are extremely difficult to obtain experimentally. Cell-scale simulations can provide insight into the physical mechanisms occurring and suggest appropriate macroscopic continuum models. Furthermore, critical high shear regions in VADs are often characterized by dimensions on the order of a few tens of microns, such as in bearings and at rotor tips. Modeling blood damage in such regions is crucial; yet the small length scales lead to breakdown in homogeneous blood models, and cell-scale simulations become necessary.

2. Methods for modeling flows with dynamic interfaces. There are three primary challenges to address when numerically modeling flows with dynamic interfaces, such as flows of RBCs. First, the numerical method must accurately resolve the complex motion of the interface in time and space. Second, the appropriate interface mechanics, such as surface tension, must be enforced. Finally, the numerical method must be computationally tractable, efficient, and scalable.

Many numerical techniques have been suggested for representing the motion and deformation of a dynamic fluid-fluid interface. In general, these methods can be distinguished by three characteristics:

- *The definition of the interface and its deformation.* The interface is either defined explicitly, also known as front-tracking, or implicitly, sometimes called front-capturing. An explicit method, through the use of marker particles or grid points, maintains the interface as a sharp discontinuity and tracks its motion. No modeling is required to define interface. An implicit scheme, which does not explicitly locate the interface, solves an additional set of field equations describing the motion of the interface. The location of the interface is usually reconstructed from the field equations.
- *The coordinate framework and discretization of the domain.* Generally, a choice is made between a Lagrangian (material) framework and an Eulerian (spatial) framework. In the Lagrangian framework, the fluid

*Supported by National Science Foundation's Information Technology Research program through grant ACI-0086093. The first author was partially supported under a Department of Energy Computational Science Graduate Fellowship. Computing resources on the HP AlphaCluster system at the Pittsburgh Supercomputing Center provided under NSF/AAB/PSC award BCS020001P.

[†]Ultrascale Simulation Lab, Department of Civil & Environmental Engineering, Carnegie Mellon University, Pittsburgh, PA 15213 (jhill@andrew.cmu.edu)

[‡]Department of Mathematical Sciences, Carnegie Mellon University, Pittsburgh, PA 15213 (noelw@cmu.edu)

[§]Ultrascale Simulation Lab, Departments of Biomedical Engineering and Civil & Environmental Engineering, Carnegie Mellon University, Pittsburgh, PA 15213 (oghattas@cs.cmu.edu)

flow is observed with a set of fluid particles that move with the flow over time. Generally, the topology of the interface is embedded in the discretization of the domain. As the interface deforms, the material points move with that deformation, maintaining a sharp interface. From a finite element perspective, large deformations may result in degenerate elements, necessitating re-discretization of the domain. In an Eulerian framework, the fluid flow is observed with a set of spatial points. Generally, a fixed discretization is used, eliminating the need for remeshing, except as increased resolution is required. However, because the interface may not be embedded in the domain discretization, the interface must be resolved through other means.

- *The coupling of the interface forces.* In a front-tracking method, the location of the interface is exactly known. Interfacial forces, such as surface tension, can be applied directly at the interface. A front-capturing method does not exactly resolve the location of the interface; thus, interfacial forces are often smeared across a finite region near the interface.

Numerical methods for dynamic interfaces usually fall into the categories of *front-tracking Lagrangian methods*, such as pure Lagrangian [1] or Arbitrary Lagrangian Eulerian [12] methods; *front-capturing Eulerian methods*, such as volume of fluid [10, 23], level set method [18, 25], and phasefield [28] methods; or *front-tracking Eulerian methods*, such as immersed boundary [19, 27], immersed interface [15], fictitious domain [8], distributed Lagrange multiplier [13], and embedded boundary [3, 11] methods.

Front-tracking Lagrangian methods have the advantages that the interface is sharply resolved, the material description is natural for elastic interfaces, and the numerics are often simplified due to the Lagrangian form of the equations. The major disadvantage, however, is in the computational geometry required to maintain quality propagating meshes as they conform to dynamic interfaces, which is particularly difficult on highly parallel computers [1]. The absence of any reported 3D parallel Lagrangian implementations for the flow of elastic bodies undergoing large translations and rotations attests to these difficulties.

Front-capturing Eulerian methods are attractive for interfaces and boundaries undergoing large deformations and topological changes. The primary advantage is their ability to capture large deformations of the interface without requiring the grid to be re-discretized. Rather than explicitly tracking the interface, these methods reconstruct it as an isocontour of a field variable. This results in the cleanest parallel implementation of the three classes of methods; but due to the lack of explicit treatment, interfacial forces are generally smeared over a small region surrounding the interface. Moreover, elasticity is an inherently Lagrangian quantity, requiring knowledge of the reference configuration of the body relative to its current position, so special techniques must be devised to incorporate elastic interfaces.

Front-tracking Eulerian methods occupy an intermediate position between explicit Lagrangian and implicit Eulerian methods. The interface is explicitly tracked using a Lagrangian representation, and embedded within a fixed-mesh Eulerian problem domain that does not conform to the interface motion. Interfacial forces, such as surface tension, are coupled between the interface and the domain as body forces applied at grid points in the vicinity of the interface. Computational geometry is not as complex as for Lagrangian methods, but not as straightforward as in front-capturing Eulerian methods due to the need to explicitly track the interface, which complicates parallel implementations.

We conclude that for problems of simulating flows with numerous elastic membranes undergoing large rotations and translations, front-capturing Eulerian methods offer the most straightforward path to achieving large-scale parallelism. The major barriers that must be overcome are development of stable Eulerian models for flow-membrane interaction and efficient methods for their numerical approximation and parallel implementation. Our approach is based on a phasefield model to distinguish interiors and exteriors of cells, a phasefield Eulerian model for elastic interfaces, discontinuous/continuous Galerkin schemes for the numerical approximation, and operator split/domain decomposition solvers. In this note we give an overview of the methods and provide preliminary scalability and performance data on up to 64 processors of the AlphaServer cluster at the Pittsburgh Supercomputing Center for some model 2D and 3D problems. A longer article will contain simulations with multiple interacting cells on a large configuration of the machine. Due to the Eulerian formulation, simulating flows of multiple cells on multiple processors presents no special difficulties other than longer run times.

3. A phasefield Eulerian model for flows with elastic membranes. In this section we give an overview of an Eulerian phasefield continuum mechanics model for the flow of viscous incompressible fluids enclosed by elastic membranes, embedded with another viscous incompressible fluid. Details on the derivation of the model and an analysis of its stability can be found in [9].

3.1. The phase variable. The phase variable, $\phi(x, t)$, an order parameter, is defined for a two-phase system of incompressible fluids such that

$$\phi(x, t) = \begin{cases} +1 & x \in \Omega_A(t) \\ 0 & x \in \Gamma(t) \\ -1 & x \in \Omega_B(t) \end{cases}, \quad (3.1)$$

where Ω_A and Ω_B are the regions occupied by fluid A and fluid B and Γ is the interface between Ω_A and Ω_B . For immiscible fluids, the phase variable uniquely defines the density, and similarly other material properties, at every point (x, t) in Ω as

$$\rho(x, t) = \frac{1 + \phi(x, t)}{2} \rho_A + \frac{1 - \phi(x, t)}{2} \rho_B, \quad (3.2)$$

where ρ_A and ρ_B are the densities of fluids A and B, respectively.

As defined, $\phi(x, t)$ is an Eulerian (or spatial) quantity, dependent on the spatial coordinate x and time t . The equivalent Lagrangian (or material) description, $\Phi(X) = \phi(x(X, t), t)$, is independent of time; therefore, the material time derivative is zero, or $\Phi' = 0$. The equivalent Eulerian expression is

$$\phi_t + v \cdot \nabla \phi = 0. \quad (3.3)$$

Physically, this equation describes the phase at every spatial point $x \in \Omega$ at time t for a given velocity field v .

3.2. Balance of momentum and mass. The balance of linear momentum and mass for incompressible, Newtonian fluids requires that

$$\rho(v_t + (v \cdot \nabla)v) - \operatorname{div}(pI + \mu D(v)) + T = \rho f, \quad (3.4)$$

$$\rho_t + \nabla \cdot (\rho v) = 0, \quad (3.5)$$

where v is the fluid velocity, p the fluid pressure, f an externally applied force, μ the fluid viscosity, $D(v) = \frac{1}{2}(\nabla v + (\nabla v)^T)$ is the stretching tensor of the velocity field, and T is the Cauchy stress of the elastic membrane. Substituting the expression (3.2) for density in terms of phase variable into the mass equation (3.5), and making use of the conservation of phase relation (3.3), gives the condition

$$\operatorname{div}(v) = 0 \quad (3.6)$$

Thus we may take (3.3), (3.4), and (3.6) as the governing equations.

3.3. The elastic membrane. In this section we describe the model for the elastic membrane and its incorporation into the balance of momentum equation (3.4). The Cauchy stress for an elastic membrane is expressed as

$$T_s = \frac{4}{J_s} R_s \mathbb{C}(E_s) R_s^T \quad (3.7)$$

where R_s and E_s are the rotation and strain tensors of the membrane and \mathbb{C} is the elasticity tensor. In this work, we restrict ourselves to isotropic elastic membranes, for which the constitutive assumption is that

$$\mathbb{C}(E_s) = \alpha E_s + \beta \operatorname{tr}(E_s) I,$$

where α and β are the Lamé parameters. The phase field approximation for the Cauchy stress in (3.7) is

$$T \simeq \frac{4}{J} R_s \mathbb{C}(E_s) R_s^T \delta,$$

where $\delta = |\nabla_X \phi_r(X)| = |F^T \nabla_x \phi(x)|$ localizes the stress to the interface. For incompressible fluids, $J = \det(F) = 1$. To avoid the explicit computation of δ , it can be absorbed into R_s and E_s as $\check{R}_s = R_s \delta^{1/4}$ and $\check{E}_s = E_s \delta^{1/2}$. Therefore, the membrane stress becomes

$$T \simeq 4 \check{R}_s \mathbb{C}(\check{E}_s) \check{R}_s^T$$

and the equations for the evolution of the membrane rotations and strain (under small strain assumptions) are

$$\begin{aligned} \dot{\check{R}}_s &= W(v) \check{R}_s \\ \dot{\check{E}}_s &= \check{R}_s^T D(v) \check{R}_s, \end{aligned}$$

where $W(v) = \frac{1}{2}(\nabla v - (\nabla v)^T)$ is the skew part of the velocity gradient tensor. Appropriate initial conditions for an initially unstrained membrane are $R_s(0) = (I - N \otimes N)$ and $E_s(0) = 0$.

3.4. Summary of the governing equations. The full system of equations describing the phase field model for viscous incompressible flow with elastic membranes can be summarized by

$$\begin{aligned} \rho(\phi) (v_t + (v \cdot \nabla) v) - \operatorname{div} (pI + \mu(\phi)D(v) + 4\check{R}_s\mathbb{C}(\check{E}_s)\check{R}_s^T) &= \rho(\phi) f \\ \operatorname{div}(v) &= 0 \\ \phi_t + v \cdot \nabla \phi &= 0 \\ \check{R}_{s,t} + (v \cdot \nabla)\check{R}_s &= W(v)\check{R}_s, \\ \check{E}_{s,t} + (v \cdot \nabla)\check{E}_s &= \check{R}_s^T D(v)\check{R}_s, \end{aligned} \quad (3.8)$$

with appropriate boundary and initial conditions, and with rotation and strain initializations given in terms of the initial phase variable by

$$\begin{aligned} \check{R}_s(0) &= (I - N \otimes N) |\nabla_x \phi(0)|^{1/4} \\ \check{E}_s(0) &= 0. \end{aligned}$$

3.5. The weak forms of the governing equations. To affect a numerical approximation of the governing equations (3.8), we first write their weak forms. For the balance of linear momentum (3.4) and incompressibility (3.6) equations, we seek $v : (0, T] \times \Omega \rightarrow \mathbb{R}^d$, $p : (0, T] \times \Omega \rightarrow \mathbb{R}$ such that

$$\begin{aligned} \int_{\Omega} [\rho(\phi) (v_t + (v \cdot \nabla)v) \cdot w + p \operatorname{div}(w) + \mu(\phi)D(v) \cdot D(w) + T \cdot D(w)] d\Omega &= \int_{\Omega} \rho f \cdot w d\Omega + \int_{\partial\Omega_N} g \cdot w ds \quad \forall w \in \mathcal{V} \\ \int_{\Omega} \operatorname{div}(v) q d\Omega &= 0 \quad \forall q \in P \end{aligned} \quad (3.9)$$

where w and q are test functions. For the phase evolution equation (3.3), we seek $\phi : (0, T] \times \Omega \rightarrow \mathbb{R}$ such that

$$\begin{aligned} \int_{\Omega} \phi \psi d\Omega \Big|_{t=0}^T - \int_0^T \int_{\Omega} \phi (\psi_t + v \cdot \nabla \psi) d\Omega dt \\ + \int_0^T \int_{\partial\Omega_{out}} \phi \psi v \cdot n ds dt = - \int_0^T \int_{\partial\Omega_{in}} \phi_{in} \psi v \cdot n ds dt, \quad \forall \psi \end{aligned} \quad (3.10)$$

where $\partial\Omega_{out} = \{s \in \partial\Omega \mid v \cdot n \geq 0\}$, $\partial\Omega_{in} = \{s \in \partial\Omega \mid v \cdot n < 0\}$, and ψ is the test function. Similar weak forms can be derived for the strain and rotation evolution equations.

4. Numerical scheme. In this section, we give a numerical scheme for solving the coupled system of momentum, mass, phase field, strain, and rotation equations in (3.8). We choose to lag the velocity in the convective terms of the momentum and phase equations so that (1) the momentum equation becomes linear in v and (2) the momentum and phase equations decouple. In addition, the velocity field in the rotation equation is also lagged. This choice decouples the phase and rotation equations from the momentum equation; however, the strain equation remains strongly coupled to the momentum equation. The resulting algorithm is depicted in Figure 4.1 and can be summarized as follows:

1. Solve the phase equation using the discontinuous Galerkin method in both space and time. Given the solutions from the previous time step $(\phi_h^{n-1}, v_h^{n-1})$ or the initial conditions, compute the approximation of ϕ on every spatial element for the (t^{n-1}, t^n) time element as $\phi_h \in P_k \otimes R_h$,

$$\begin{aligned} \int_K \phi_h(t^n) \psi_h(t^n) - \int_{t^{n-1}}^{t^n} \int_K \phi_h ((\psi_h)_t + v^{n-1} \cdot \nabla \psi_h) \\ + \int_{t^{n-1}}^{t^n} \int_{\partial K} \left((v^{n-1} \cdot n)^+ \phi_h + (v^{n-1} \cdot n)^- \phi_{h-} \right) \psi_h \\ = \int_K \phi_{h-}(t^{n-1}) \psi_h(t^{n-1}). \end{aligned} \quad (4.1)$$

for all $\psi_h \in P_k \otimes R_h$, where P_k is the set of orthonormal polynomials of degree k . Stability arguments [9] dictate that ϕ is approximated by quartic polynomials.

2. Mean viscosity and density $\bar{\rho}$ and $\bar{\mu}$ are defined as

$$\bar{\rho} = \frac{1}{\tau} \int_{t^{n-1}}^{t^n} \rho(\phi_h)$$

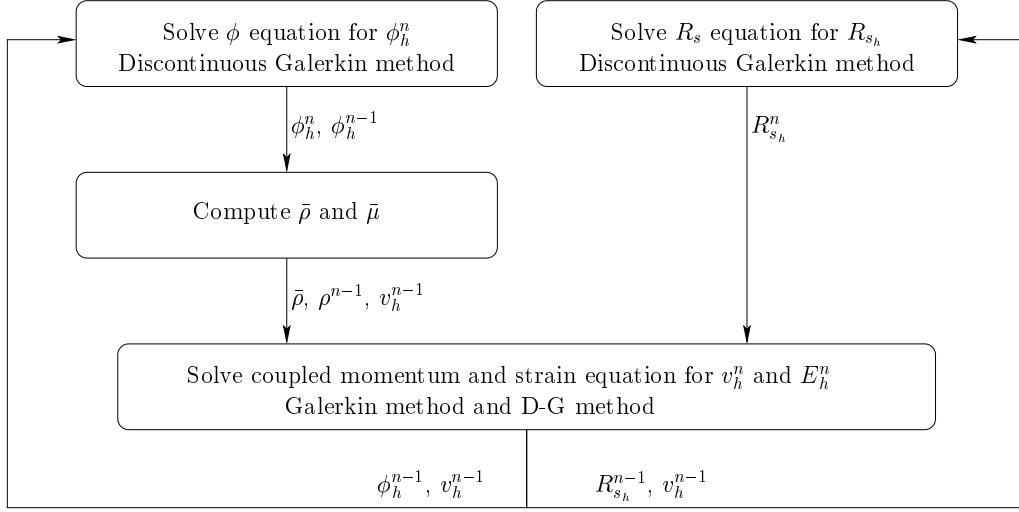


FIG. 4.1. The solution methodology for modeling the motion of two fluids separated by an elastic membrane. Lagging the velocity in the convective terms of all four systems of equations decouples the phase equation and the rotation from the momentum and strain equations.

and

$$\bar{\mu} = \frac{1}{\tau} \int_{t^{n-1}}^{t^n} \mu(\phi_h),$$

where again this approximation is dictated by stability arguments.

3. Solve the rotation equation using the discontinuous Galerkin method in both space and time. Knowing the solutions from the previous time step $(\check{R}_h^{n-1}, v_h^{n-1})$, the approximation of \check{R} on every spatial element for the (t^{n-1}, t^n) time element is computed as $\check{R}_h \in P_k \otimes \mathfrak{R}_h$,

$$\begin{aligned} \int_K \check{R}_h(t^n) S_h(t^n) - \int_{t^{n-1}}^{t^n} \int_K \check{R}_h ((S_h)_t + (v^{n-1} \cdot \nabla) S_h) + W(v^{n-1}) \check{R}_h \cdot S_h \\ + \int_{t^{n-1}}^{t^n} \int_{\partial K} \left((v^{n-1} \cdot n)^+ \check{R}_h + (v^{n-1} \cdot n)^- \check{R}_{h-} \right) S_h \\ = \int_K \check{R}_{h-}(t^{n-1}) S_h(t^{n-1}) \end{aligned} \quad (4.2)$$

for all $S_h \in P_k \otimes \mathfrak{R}_h$, where again P_k is the set of orthonormal polynomials of degree k . For simplicity, the s subscript has been neglected.

4. Finally, given the solutions from the previous time step $(\phi_h^{n-1}, v_h^{n-1})$ and the current solutions ϕ_h^n and \check{R}_h^n , solve the coupled momentum and strain equations. The momentum equation is approximated by the standard Galerkin method in space and discretized by the backward Euler method in time. Therefore, we seek an approximation of v^n, p^n on every element as $(v_h^n, p_h^n) \in V_h \times P_h$,

$$\begin{aligned} \int_{\Omega} \left[\rho(\phi_h^{n-1}) \left(\frac{v_h^n - v_h^{n-1}}{\tau} + (v^{n-1} \cdot \nabla) v_h^n \right) \cdot w_h + p_h \operatorname{div}(w_h) \right] d\Omega \\ + \int_{\Omega} \left[\bar{\mu} D(v_h^n) \cdot D(w_h) + 4\check{R}_{s_h}^n \mathbb{C}(\check{E}_{s_h}^n) (\check{R}_{s_h}^n)^T \cdot D(w_h) \right] d\Omega \\ = \int_{\Omega} \bar{p} f^{n+1/2} \cdot w_h d\Omega + \int_{\partial\Omega_N} g^{n+1/2} \cdot w_h ds, \\ \int_{\Omega} \operatorname{div}(v_h^n) q_h d\Omega = 0 \end{aligned} \quad (4.3)$$

for all $w_h \in V_h, q_h \in P_h$. We use the Taylor-Hood element (quadratic velocity, linear pressure). The strain equation is discretized in space and time by the discontinuous Galerkin method. Thus, we seek a solution

$\check{E}_h \in \mathcal{F}_h \subset \mathcal{F}$ on each space-time element $(t^{n-1}, t^n) \times K$ such that

$$\begin{aligned} & \int_K \check{E}_h(t^n) F_h(t^n) - \int_{t^{n-1}}^{t^n} \int_K \check{E}_h ((F_h)_t + (v^{n-1} \cdot \nabla) F_h) \\ & + \int_{t^{n-1}}^{t^n} \int_{\partial K} \left((v^{n-1} \cdot n)^+ \check{E}_h + (v^{n-1} \cdot n)^- \check{E}_{h-} \right) F_h \\ & - \int_{t^{n-1}}^{t^n} \int_{\partial K} \left(\check{R}^{Tn} D(v^n) \check{R}^n \cdot F_h \right) = \int_K \check{E}_{h-}(t^{n-1}) F_h(t^{n-1}) \end{aligned} \quad (4.4)$$

for all $F_h \in \mathcal{F}$. Again, for brevity, the s subscript has been neglected. The equations 4.3 and 4.4 form a coupled system of linear equations in the velocity, pressure, and strain unknowns.

5. Parallel solution. In the previous section, we have described a numerical scheme for a phase field model of the interaction of dynamic elastic membranes with viscous incompressible fluids. The combination of phase field interface capturing method, Eulerian elastic membrane model, and discontinuous Galerkin approximation of the evolution equations for phase, rotation, and strain field variables leads to a method that permits discretization on a fixed grid without explicit resolution of the interface. This affords a straightforward parallel implementation; in our case we use the parallel data structures, linear Krylov solvers, and domain decomposition preconditioners from the parallel numerical library PETSc [2].

Discontinuous Galerkin approximation of the phase, rotation, and strain evolution equations leads to well-conditioned linear systems. Because the phase (4.1) and rotation (4.2) linear systems are well-conditioned, we either use no preconditioning, or if necessary invoke the additive Schwarz preconditioner from the PETSc library with minimal overlap and fill. Krylov solution of these two systems is affected with PETSc's implementation of either GMRES, BiCGSTAB, or TFQMR. Performance results presented in Table 5.1 illustrate that typically just a handful of Krylov iterations are required per time step for the evolution equations for phase and rotation, in this case around 4. Moreover, the number of iterations is seen to be independent of mesh size and number of processors for a range of 1 to 64 processors, with isogranular increase in problem size. We have observed this algorithmic scalability for a variety of problems.

While iterative solution of the discontinuous Galerkin-discretized evolution equations scales optimally, it is well known that Galerkin approximation of the momentum and incompressibility equations for viscous incompressible fluids typically results in ill-conditioned linear systems, which require aggressive preconditioning. Moreover, here the fluid velocity/pressure unknowns are strongly coupled with the strain unknowns (which is why we do not decouple the two systems). Because of disparate elastic and viscous properties, this coupled system can be very ill-conditioned; moreover, large numbers of Navier-Stokes iterations can drag along the strain computation during the system solve. This is problematic, since strains are tensor quantities, and they are approximated by piecewise quartic polynomials, both of which lead to large systems and additional work if iterated too many times. Therefore, it is crucial to precondition the coupled Navier-Stokes–strain evolution linear system in a way that exploits the structure and favorable conditioning of the strain problem and is effective in reducing the number of iterations.

In the remainder of this section we describe a Schur complement-type preconditioner displaying these properties. The coupled momentum, incompressibility, and strain equations for fluid flow with an elastic membrane can be written in block form as

$$\begin{bmatrix} \mathbf{A}_{uu} & \mathbf{A}_{uE} \\ \mathbf{A}_{Eu} & \mathbf{A}_{EE} \end{bmatrix} \begin{Bmatrix} \mathbf{u} \\ \check{\mathbf{E}}_s \end{Bmatrix} = \begin{Bmatrix} \mathbf{f}_u \\ \mathbf{f}_E \end{Bmatrix} \quad (5.1)$$

where \mathbf{u} represents the velocity and pressure unknowns, and $\check{\mathbf{E}}_s$ the strain unknowns. An exact factorization of the matrix \mathbf{A} is

$$\mathbf{A} = \begin{bmatrix} \mathbf{A}_{uu} & \mathbf{A}_{uE} \\ \mathbf{A}_{Eu} & \mathbf{A}_{EE} \end{bmatrix} = \begin{bmatrix} \mathbf{S} & \mathbf{A}_{uE} \\ \mathbf{0} & \mathbf{A}_{EE} \end{bmatrix} \begin{bmatrix} \mathbf{I} & \mathbf{0} \\ \mathbf{A}_{EE}^{-1} \mathbf{A}_{uE} & \mathbf{I} \end{bmatrix}$$

where $\mathbf{S} = \mathbf{A}_{uu} - \mathbf{A}_{uE} \mathbf{A}_{EE}^{-1} \mathbf{A}_{Eu}$ is the Schur complement of \mathbf{A}_{uu} in \mathbf{A} . We can write the preconditioner for \mathbf{A} symbolically as

$$\mathbf{P} = \begin{bmatrix} \mathbf{I} & \mathbf{0} \\ -\tilde{\mathbf{A}}_{EE}^{-1} \mathbf{A}_{uE} & \mathbf{I} \end{bmatrix} \begin{bmatrix} \tilde{\mathbf{S}}^{-1} & -\tilde{\mathbf{S}}^{-1} \mathbf{A}_{uE} \tilde{\mathbf{A}}_{EE}^{-1} \\ \mathbf{0} & \tilde{\mathbf{A}}_{EE}^{-1} \end{bmatrix}$$

where $\tilde{\mathbf{S}}^{-1}$ and $\tilde{\mathbf{A}}_{EE}^{-1}$ are approximate inverses of \mathbf{S} and \mathbf{A}_{EE} . A convenient and inexpensive choice for $\tilde{\mathbf{A}}_{EE}$ is to include just element contributions from the discontinuous Galerkin approximation and neglect face contributions.

TABLE 5.1

Parallel performance and isogranular scalability of coupled flow-elastic membrane solver. Problem solved is 2D elastic fluid-filled capsule falling under gravity. Preconditioner is additive Schwarz with ILU(1) and $\beta = 1$ overlap. PEs is number of processors; Elements refers to number of Taylor-Hood or discontinuous Galerkin elements; Time steps is number of time steps for an entire simulation; DOF is number of unknowns for phase (ϕ), rotation (R), strain (equal to R), and velocity/pressure (N-S) variables; Iterations are average number of GMRES iterations for the phase system (ϕ), GRMRES iterations for the rotation system (R), and TFQMR iterations for the coupled strain-momentum-continuity system (N-S); and Time is seconds of wallclock to carry out the specified number of time steps.

PEs	Elements Time Steps	DOF		iterations		Time (s)
		ϕ R N-S	ϕ	R	N-S	
1	8 x 8	1,024	1.34	1,36	20.21	32
	38	2,467				
		659				
4	16 x 16	4,096	3.93	3.97	40.85	97
	75	16,384				
		2,467				
16	32 x 32	16,384	4.20	4.20	72.40	335
	150	65,536				
		9,539				
32	45 x 45	32,400	4.03	4.06	112.90	919
	225	129,600				
		18,678				
64	64 x 64	65,536	4.05	4.13	137.62	1522
	300	262,144				
		37,507				

Recall from (4.4) that the discrete form for \mathbf{A}_{EE} is given implicitly by

$$\begin{aligned} \mathbf{F}^T \mathbf{A}_{EE} \mathbf{E}_s &= \int_K \check{E}_h(t^n) F_h(t^n) - \int_{t^{n-1}}^{t^n} \int_K \check{E}_h(v^{n-1} \cdot \nabla) F_h \\ &\quad + \int_{t^{n-1}}^{t^n} \int_{\partial K} \left((v^{n-1} \cdot n)^+ \check{E}_h + (v^{n-1} \cdot n)^- \check{E}_{h-} \right) F_h. \end{aligned}$$

Therefore, the approximation for $\tilde{\mathbf{A}}_{EE}$ is taken as

$$\mathbf{F}^T \tilde{\mathbf{A}}_{EE} \mathbf{E}_s = \int_K \check{E}_h(t^n) F_h(t^n) - \int_{t^{n-1}}^{t^n} \int_K \check{E}_h(v^{n-1} \cdot \nabla) F_h.$$

Because only element contributions are considered and because the spatial and temporal approximations for the strain are discontinuous, $\tilde{\mathbf{A}}_{EE}$ is block-diagonal, with blocks corresponding to (quartic) elements. Therefore, $\mathbf{A}_{uE} \tilde{\mathbf{A}}_{EE}^{-1} \mathbf{A}_{Eu}$ has the same sparsity structure as $\tilde{\mathbf{A}}_{uu}$ and is assembled across processors in the usual way. Another approximation we make in the preconditioner is to replace the saddle point matrix \mathbf{A}_{uu} corresponding to velocity and pressure unknowns with its pressure-stabilized form $\tilde{\mathbf{A}}_{uu}$, i.e. the $\mathbf{0}$ in the (2,2) block is replaced by the scaled discrete Laplacian $\beta h^2 \Delta_h$. This yields a matrix that is more amenable to standard domain decomposition preconditioners.

Finally, we employ an additive Schwarz preconditioner from the PETSc library to approximate $\tilde{\mathbf{S}}^{-1}$, using generous overlap and fill for particularly difficult problems. Performance results suggest that our preconditioner for the coupled membrane–momentum–mass system (5.1) effectively neutralizes the relative stiffness of the membrane; that is, the iteration complexity of the preconditioned system is the same with or without the membrane, as can be seen by comparing the growth in *N-S iterations* of the membrane (Table 5.1) and no-membrane (Table 5.2) cases. In either case, the iteration count increases with the square root of problem size. Although the number of iterations does depend on problem size, this is expected since we are using a single-level domain decomposition preconditioner for the Navier-Stokes component. This can be overcome by implementing a multilevel preconditioner, which we have not yet done in anticipation of a forthcoming public release of a robust parallel algebraic multigrid solver. In any case, the preconditioner appears to effectively treat ill-conditioning due to mixing of fluid and elastic properties in the coupled system.

TABLE 5.2

Parallel performance and isogranular scalability of multifluid flow solver without membrane. All column headings similar to those in table 5.1.

PEs	Elements Time Steps	DOF		iterations		Time (s)
		ϕ N-S	ϕ	N-S		
1	16 x 16	4,096	2.96	10.28	25	
	75	2,467				
4	32 x 32	16,384	4.11	23.57	72	
	150	9,539				
8	45 x 45	32,400	4.90	30.76	136	
	225	18,678				
16	64 x 64	65,536	4.34	44.34	228	
	300	37,507				
32	91 x 91	132,496	4.66	60.88	467	
	450	75,442				

6. A two-dimensional example. To illustrate the effect of the elastic membrane, we simulate the flow of a denser, more viscous cell with and without an elastic membrane through a notched channel. Consider the spatial domain $\Omega = \{(x, y) \mid -1.0 \leq x \leq 1.0, -0.5 \leq y \leq 0.5\}$ containing two immiscible fluids, \mathcal{F}_{bulk} and \mathcal{F}_{cell} , with material properties

$$\begin{aligned} \mu_{bulk} &= 1.0, & \rho_{bulk} &= 1.0, \\ \mu_{cell} &= 2.0, & \rho_{cell} &= 2.0, \end{aligned}$$

as shown in Figure 6.1. Traction-free, or Neumann, boundary conditions are assumed on $\partial\Omega_{out}$; Dirichlet boundary conditions are applied to the remainder of the boundary. Initially, the fluids are at rest; however, a Poiseuille flow profile, $v_x = (0.25 - y^2)$, is introduced through Dirichlet boundary conditions on $\partial\Omega_{in}$. We examine the time domain $t \in [0, 3]$.

In these examples, the spatial domain Ω is discretized into 2,720 quadrilateral elements with element length $h = 0.025$. Taylor-Hood elements, quadratic in v and linear in p , approximate v_h and p_h , respectively; biquartic elements approximate ϕ_h , R_h and E_h . The time domain is discretized into 4,800 time steps.

Figure 6.2 demonstrates the evolution of the phase variable through time. As expected, in the absence of an elastic membrane at the fluid-fluid interface, the velocity profile dictates the shape of the cell. Figure 6.3 illustrates the effect of the elastic membrane, with elastic constants

$$\alpha = \beta = 2.5 \times 10^4,$$

on the shape of the deforming cell. The effect of the elastic membrane is readily apparent when comparing the shape of the cell during the simulation to that in Figure 6.2. The elasticity of the membrane dictates the shape of the cell, rather than the velocity profile.

7. A three-dimensional example. The primary motivation for modeling the fluid-fluid interface with a front-capturing method, such as the phase field method, is to avoid the numerical and geometric difficulties associated with remeshing, especially in three-dimensions. We illustrate the flexibility of the phasefield method and its extensibility by the following three-dimensional example.

Consider a spatial domain $\Omega = \{(x, y, z) \mid -1.5 \leq x, y, z \leq 1.5\}$, again containing two immiscible fluids, \mathcal{F}_{bulk} and \mathcal{F}_{drop} , with material properties

$$\begin{aligned} \mu_{bulk} &= 1.0, & \rho_{bulk} &= 1.0, \\ \mu_{drop} &= 2.0, & \rho_{drop} &= 2.0. \end{aligned}$$

Initially, fluid \mathcal{F}_{drop} is of spherical shape with radius 0.5 centered at $(0, 0, 0.75)$. Dirichlet, or fixed, boundary conditions were applied to $\partial\Omega$; initially, the fluids were at rest. We study the effect of a gravity body force acting on the domain over $t \in [0, 10]$.

The spatial domain Ω was discretized into $16 \times 16 \times 16$ hexahedral elements. Again, v_h and p_h are approximated with Taylor-Hood elements; triquartic elements approximate ϕ_h . The time domain was discretized into 1000 time steps. Figure 7.1 illustrates the evolution of the level set of the phase variable with time. As expected, the evolution of the phase variable is an axisymmetric form of the two-dimensional example.

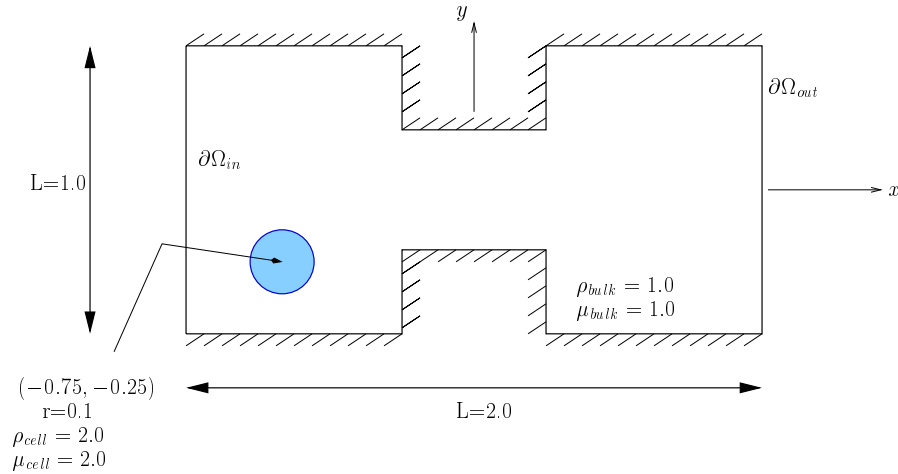


FIG. 6.1. The schematic of the geometry and material properties for the simulation of a cell, both with and without an elastic membrane, flowing through a notched channel.

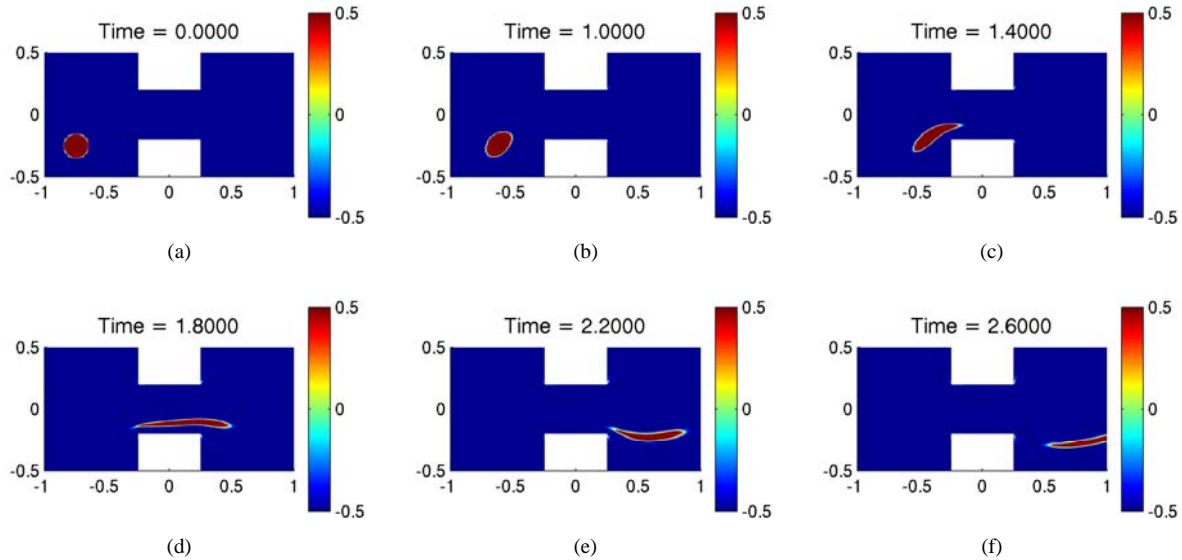


FIG. 6.2. The evolution of the phase function for a cell flowing through a notched channel at times (a) $t = 0.0$, (b) $t = 1.0$, (c) $t = 1.4$, (d) $t = 1.8$, (e) $t = 2.2$ and (f) $t = 2.6$. In this example, there is no elastic membrane present at the interface.

REFERENCES

- [1] J. ANTAKI, G. BLELLOCH, O. GHATTAS, I. MALCEVIC, G. MILLER AND N. WALKINGTON, *A parallel dynamic-mesh Lagrangian method for simulation of flows with dynamic interfaces*, in Proceedings of SC2000, Dallas, TX, Nov. 4-10, 2000.
- [2] S. BALAY, K. BUSCHELMAN, W. D. GROPP, D. KAUSHIK, M. KNEPLEY, L. C. MCINNES, B. F. SMITH, AND H. ZHANG, *PETSc home page*. <http://www.mcs.anl.gov/petsc>, 2001.
- [3] G. BIROS, L. YING, AND D. ZORIN, *A fast solver for the Stokes equations with distributed forces in complex geometries*, Journal of Computational Physics, 193 (2004), pp. 317-348.
- [4] G. BURGEEEN, J. ANTAKI AND B. GRIFFITH, *A design improvement strategy for axial blood pumps using computational fluid dynamics*, ASAIO Journal, 42 (1996), pp. M354-M360.
- [5] G.W. BURGEEEN AND J.F. ANTAKI, *CFD-based design optimization of a three-dimensional rotary blood pump*, in Proceedings of the Sixth AIAA/NASA/ISSMO Symposium on Multidisciplinary Analysis and Optimization, AIAA, September 1996.
- [6] C.D. EGGLETON AND A.S. POPEL, *Large deformation of red blood cell ghosts in a simple shear flow*, Physics of Fluids, 10 (1998), pp. 1834-1845.
- [7] J. GLIMM, X.-L. LI, Y.-J. LIU, AND Z. XU, *Conservative front tracking with improved accuracy*, SIAM Journal on Numerical Analysis, 41 (2003), pp. 1926-1947.
- [8] R. GLOWINSKI, T. PAN, AND J. PERIAUX, *Fictitious domain methods for incompressible viscous flow around moving rigid bodies*, in The Mathematics of Finite Elements and Applications, John Wiley & Sons, 1996, pp. 155-174.
- [9] J. HILL, *Phase Field Methods for Flows of Elastic Membranes*, Ph.D. thesis, Carnegie Mellon University (2004).
- [10] C.W. HIRT AND B.D. NICHOLS, *Volume of fluid (VOF) method for the dynamics of free boundaries*, Journal of Computational Physics, 39

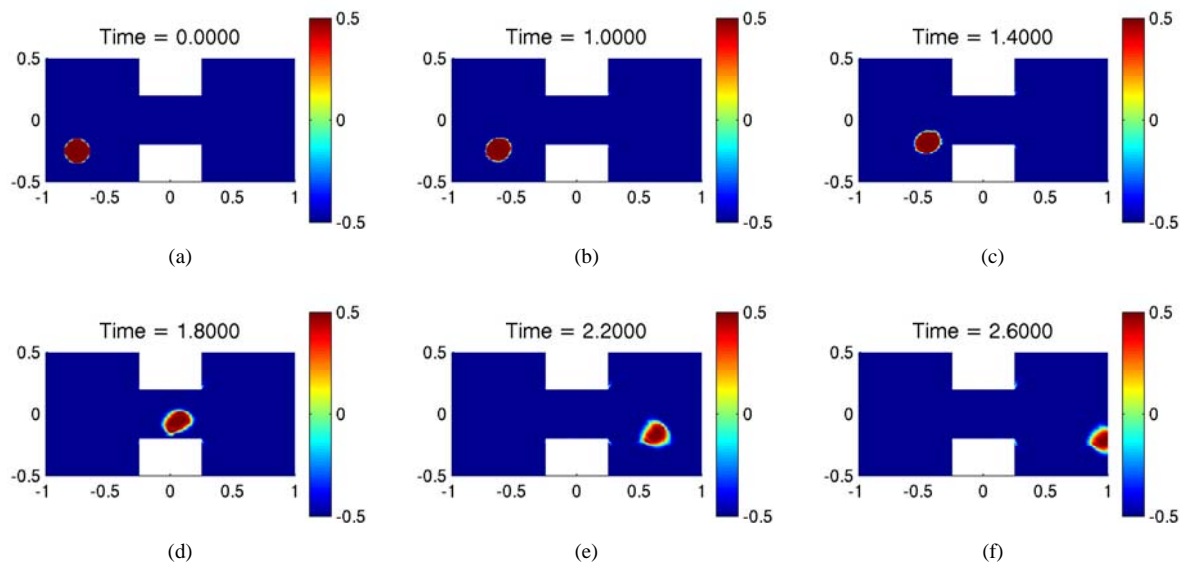


FIG. 6.3. The evolution of the phase function for a cell flowing through a notched channel. In this example, there is an elastic membrane present at the interface.

- (1981), pp. 201-225.
- [11] H. JOHANSEN AND P. COLELLA, *A Cartesian grid embedded boundary method for Poisson's equation on irregular domains*, Journal of Computational Physics, 147 (1998), pp. 60-85.
- [12] A. JOHNSON AND T. TEZDUYAR, *3D simulation of fluid-particle interactions with the number of particles reaching 100*, Computer Methods in Applied Mechanics and Engineering, 145 (1997), pp. 301-321.
- [13] D. D. JOSEPH, *Interrogations of Direct Numerical Simulation of Solid-Liquid Flows*, http://www.efluids.com/efluids/books/efluids_books.htm.
- [14] G. KARYPIS, K. SCHLOEGEL, AND V. KUMAR, *ParMETIS 3.0*. <http://www-users.cs.umn.edu/~karypis/metis/parmetis>.
- [15] R.J. LEVEQUE AND Z. LI, *The immersed interface method for elliptic equations with discontinuous coefficients and singular sources*, SIAM Journal on Numerical Analysis, 31 (1994), pp. 1019-1044.
- [16] D. LOGHIN, *Schur complement preconditioners for the Navier-Stokes equations*, 5th IMACS Conference on Iterative Methods in Scientific Computing, May 2001.
- [17] Y. NAVOT, *Elastic membranes in viscous shear flow*, Physics of Fluids, 10 (1998), pp. 1819-1833.
- [18] S. OSHER AND J.A. SETHIAN, *Fronts propagating with curvature dependent speed: Algorithms based in Hamilton-Jacobi formulations*, Journal of Computational Physics, 79 (1988), pp. 12-49.
- [19] C.S. PESKIN, *Numerical analysis of blood flow in the heart*, Journal of Computational Physics, 25 (1977), pp. 220-252.
- [20] C. POZRIKIDIS, *Finite deformation of liquid capsules enclosed by elastic membranes in simple shear flow*, Journal of Fluid Mechanics, 297 (1995), pp. 123-152.
- [21] C. POZRIKIDIS, *Hydrodynamics of liquid capsules enclosed by elastic membranes*, In Computational Modelling in Biological Fluids, L. Fauci and S. Gueron (Eds.), Minneapolis, MN, 2000.
- [22] C. POZRIKIDIS, *Numerical simulation of the flow-induced deformation of red blood cells*, Annals of Biomedical Engineering, 31 (2003), pp. 1194-1205.
- [23] R. SCARDOVELLI AND S. ZALESKI, *Direct numerical simulation of free-surface and interfacial flow*, Annual Review of Fluid Mechanics, 31 (1999), pp. 567-603.
- [24] T.W. SECOMB, R. SKALAK, N. OZKAYA, AND J.F. GROSS, *Flow of axisymmetric red blood cells in narrow capillaries*, Journal of Fluid Mechanics, 163 (1986), pp. 405-423.
- [25] J.A. SETHIAN, *Level set methods: Evolving interfaces in geometry, fluid mechanics, computer vision, and materials science*, Cambridge University Press, (1996).
- [26] W. SHYY, *Computational modeling for fluid flow and interfacial transport*, Elsevier Science Publishers, Amsterdam, (1994).
- [27] S.O. UNVERDI AND G. TRYGGVASON, *A front tracking method for viscous, incompressible, multi-fluid flows*, Journal of Computational Physics, 100 (1992), pp. 25-37.
- [28] A.A. WHEELER, W.J. BOETTINGER AND G.B. MCFADDEN, *Phase field model for isothermal phase transitions in binary alloys*, Physical Review A, 45 (1992), pp. 7424-7439.

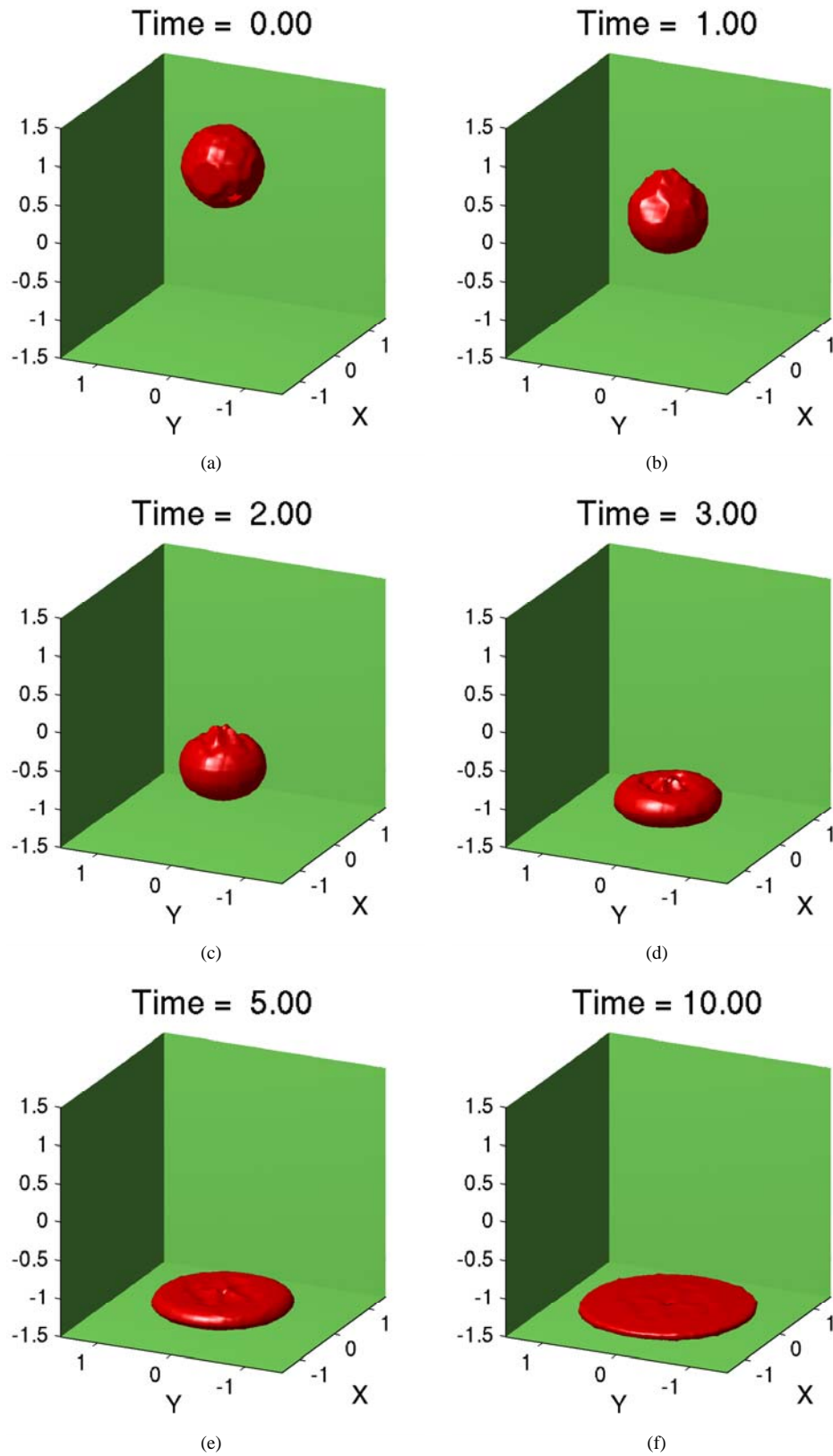


FIG. 7.1. The isosurface, $\phi = 0$, of the phase variable for a three-dimensional falling drop simulation without an elastic membrane.